JBC Papers in Press. Published on September 5, 2012 as Manuscript M112.391607
The latest version is at http://www.jbc.org/cgi/doi/10.1074/jbc.M112.391607

Crystal Structures of the scaffolding protein LGN reveal the general mechanism by which GoLoco binding motifs inhibit the release of GDP from $G\alpha_i$ subunits in G-coupled heterotrimeric proteins*

Min Jia[1,2,5], Jianchao Li[3,5], Jinwei Zhu[1,3], Wenyu Wen[1], Mingjie Zhang[3,4,*], and Wenning Wang[1,*]

[1]From Shanghai Key Laboratory of Molecular Catalysis and Innovative Materials, Department of Chemistry and Institute of Biomedical Sciences, [2]Department of Pharmacy, Fudan University, Shanghai 200433, China
[3]Division of Life Science, State Key Laboratory of Molecular Neuroscience, [4]Center of Systems Biology and Human Health, Hong Kong University of Science and Technology, Clear Water Bay, Kowloon, Hong Kong

*****Running title: *Crystal Structures of LGN GoLoco/$G\alpha_i$ Complex*

[5]These two authors contributed equally to this work

[*]Corresponding authors

Mingjie Zhang
Division of Life Science, Hong Kong University of Science and Technology
Clear Water Bay, Kowloon, Hong Kong
Tel: +852-23588709
Email : mzhang@ust.hk

Wenning Wang
Shanghai Key Laboratory of Molecular Catalysis and Innovative Materials, Department of Chemistry and Institute of Biomedical Sciences
220 Handan Road, Shanghai 200433, China
Tel : +86-21-65643985; Fax: +86-21-65641740
Email : wnwang@fudan.edu.cn,

Keyword: G protein; GoLoco; LGN; GDI; Crystal structure

Background: GoLoco (GL) motif binds to Gα and inhibits its guanine nucleotide dissociation.

Results: Crystal structures of LGN-GL3(4)/$G\alpha_{i1(3)}$ complexes reveal a "double Arg-finger"-mediated GDP recognition mechanism which is distinct from that shown in the RGS14/$G\alpha_{i1}$ complex.

Conclusion: LGN-GL/$G\alpha_i$ interaction might represent a general binding mode between GoLoco motifs and $G\alpha_i$.

Significance: Our findings shed new light on the GoLoco motif-mediated G-protein signaling regulation.

SUMMARY

GoLoco (GL) motif-containing proteins regulate G-protein signaling by binding to Gα subunit and acting as guanine nucleotide dissociation inhibitors (GDI). GLs of LGN are also known to bind GDP form of $G\alpha_{i/o}$ during asymmetric cell division. Here, we show that the C-terminal GL domain of LGN binds four molecules of $G\alpha_i$·GDP. The crystal structures of $G\alpha_i$·GDP in complex with LGN GL3 and GL4, respectively, reveal distinct GL/$G\alpha_i$ interaction features when compared to the only high-resolution structure known GL/$G\alpha_i$ interaction between RGS14 and $G\alpha_{i1}$. Only a few residues C-terminal to the conserved GL sequence are required for LGN GLs to bind to $G\alpha_i$·GDP. A highly conserved double Arg-finger sequence ("R-Ψ-D/E-D/E-Q-R") is responsible for LGN GL to bind to GDP bound to $G\alpha_i$. Together with the sequence alignment, we suggest that the LGN GL/$G\alpha_i$ interaction represents a general binding mode between GL motifs and $G\alpha_i$. We also show that LGN GLs are potent GDIs.

The α subunit of the heterotrimeric G proteins (Gα) is a critical component of the G protein signaling pathway, in which Gα cycles between the GDP and GTP bound states (1). In the canonical signaling model, ligand-mediated activation of G-protein coupled receptors (GPCR) catalyzes the exchange of GDP for GTP in binding to Gα and subsequently results in the dissociation of Gα·GTP from Gβγ heterodimer (2,3). The dissociated Gα·GTP binds to and activates downstream effectors, thus transducing signals from GPCR (4-6). Since Gα has intrinsic GTPase activity, the Gα subunit subsequently returns to the Gα·GDP form which marks the termination of the GPCR signaling. Many proteins have been discovered as regulators of the GTP- and GDP-bound forms of the Gα reaction cycle. Among these, GoLoco motif proteins were discovered to bind specifically to GDP-loaded $G\alpha_i$ or $G\alpha_o$ and inhibit the spontaneous release of GDP from Gα. These GoLoco proteins are referred to as guanine nucleotide dissociation inhibitors (GDI) (7-11).

The GoLoco motif (8,12,13) was first identified as a conserved sequence of 19 amino acids, occurring singly or as tandem repeats in a variety of signaling proteins across the animal kingdom (7). Our understanding of the molecular mechanism of the GDI function of GoLoco proteins is mainly based on the crystal structure of RGS14 GoLoco bound to $G\alpha_{i1}$·GDP (14), which shows that the conserved GoLoco motif and its variable C-terminal tail interact with the Ras-like and all-helical domains of $G\alpha_{i1}$, respectively. A so-called "arginine finger" formed by the highly conserved 'D/E-Q-R' triad in the conserved GoLoco motif extends into the GDP binding pocket and directly contacts the α- and β-phosphates of GDP (14). This structure

and the subsequent mutagenesis and structural studies (14-18) suggested an appealing hypothesis: the highly variable C-terminal sequences following the conserved GoLoco motifs and the all-helical domain of Gα subunits are likely the specificity determinants of interactions between GoLoco motifs and different Gα subunits. However, since there are no structures of GoLoco motifs in complex with Gα other than the $G\alpha_{i1}$/RGS14 complex are available to date, the above hypothesis remains untested.

LGN is a multi-domain scaffolding protein containing eight tetratricopeptide (TPR) repeats in its N-terminal region, a flexible linker sequence in the middle, and four GoLoco motifs in the C-terminal end(19,20). LGN is an evolutionarily conserved protein (Pins in *Drosophila*, and GPR1/2 in *C. elegans*) that plays crucial roles in regulating spindle orientations during asymmetric cell division (19,21), and can be considered as an example member of the multiple GoLoco motif protein family. It forms a ternary protein complex with nuclear mitotic apparatus protein NuMA (Mud in *Drosophila* and Lin5 in *C. elegans*) and cortical membrane-bound $G\alpha_{i/o}$ via its TPR repeats and GoLoco motifs, respectively (22-28). The central linker of LGN binds to the guanylate kinase domain of the DLG family scaffold protein in a phosphorylation-dependent manner(29-31). In *Drosophila* neuroblast, loss of Pins or $G\alpha_i$ affects cell polarity as well as mitotic spindle orientation (32). In mammals, overexpression or removal of LGN results in dramatic spindle rocking in metaphase and improper spindle pole organization (19,21,33). The binding of $G\alpha_i$ through the GoLoco motifs was shown to regulate the cortical localization of LGN (33). Thus the LGN GoLoco motifs can be viewed as scaffolding modules in tethering LGN's TPR repeats partners (e.g. NuMA/Mud and mInsc/Insc) to cell cortex via binding to membrane attached $G\alpha_i$. Interestingly, the GoLoco motifs of LGN can directly bind to TPR repeats intra-molecularly, thus keeping LGN in an auto-inhibited conformation (22). $G\alpha_i$·GDP binding to GoLoco motifs releases the auto-inhibited conformation of LGN and renders LGN TPR repeats capable of binding to NuMA (22,34), although the mechanistic basis of the LGN auto-inhibition is unknown.

In this study, we performed detailed biochemical and structural analyses of the interactions between LGN GoLoco motifs and $G\alpha_i$·GDP. We demonstrate that in contrast to the RGS14/$G\alpha_i$·GDP interaction, only a few residues of the highly variable sequences C-terminal to the conserved GoLoco motifs of LGN are involved in binding to $G\alpha_i$·GDP. The structures of two LGN GoLoco motifs in complex with $G\alpha_i$ reveal a "double Arg-finger" sequence ("R-Ψ-D/E-D/E-Q-R") within the GoLoco motif that is specifically involved in the GDP coordination. We further show that the LGN GoLoco/$G\alpha_i$·GDP interaction observed in this study likely represents a general mode of GoLoco motif-mediated Gα bindings. We further demonstrate that the LGN GoLoco motifs are potent GDIs. Thus the LGN GoLoco motifs can function as a Gα/LGN/NuMA/Insc scaffold as well as a regulator of Gα signaling in asymmetric cell division.

Experimental Procedures

Protein Expression and Purification

The human $G\alpha_{i3}$, $G\alpha_{i1}$, mouse LGN GL fragments were individually cloned into a modified version of pET32a vector. All the mutations were created using the standard PCR-based method and confirmed by DNA

sequencing. Recombinant proteins were expressed in *Escherichia coli* BL21 (DE3) host cells at 16 or 37 °C and were purified by using a Ni^{2+}-NTA agarose affinity chromatography followed by size-exclusion chromatography. For *in vitro* biochemical analysis, LGN GLs were expressed as the GST-fused proteins and purified by GSH-Sepharose affinity chromatography.

Isothermal Titration Calorimetry Measurements

ITC measurements were performed on an ITC200 Micro calorimeter (MicroCal) at 25 °C. All protein samples were dissolved in the buffer containing 50 mM Tris, pH 8.0, 100 mM NaCl, and 1 mM EDTA. The titrations were carried out by injecting 40 μL $G\alpha_{i3}$·GDP aliquots (0.2 mM) into LGN GLs fragments fused to the C-terminal end of thioredoxin (0.02 mM) at time intervals of 2 minutes to ensure that the titration peak returned to the baseline. The titration data were analyzed using the program Origin7.0 from MicroCal.

Fluorescence Polarization Assay

Fluorescence polarization assay were performed on a PerkinElmer LS-55 fluorimeter equipped with an automated polarizer at 25 °C. Commercial synthesized peptides were labeled with fluorescein-5-isothiocyanate (Invitrogen, Molecular Probe) at N-termini. In a typical assay, the FITC-labeled peptide (~1 μM) was titrated with binding partners in a 50 mM Tris, pH 8.0 buffer containing 100 mM NaCl, 1 mM DTT, and 1 mM EDTA. The K_D values were obtained by fitting the titration curves with the classical one-site binding model, with or without invoking the Hill coefficient model.

GST Pull-Down Assay

For GST pull-down assay, GST or GST-tagged proteins (60 μl from 1 mg/ml stock solutions) were first loaded to 40 ml GSH-Sepharose 4B slurry beads in an assay buffer (50 mM Tris, pH 8.0, 100 mM NaCl, 1 mM DTT, and 1 mM EDTA). The GST fusion protein-loaded beads were then mixed with potential binding partners, and the mixtures were incubated for 1 hr at 4 °C. After three times washing, proteins captured by affinity beads were eluted by boiling, resolved by 15% SDS-PAGE, and detected by Coomassie blue staining.

*A*nalytical *Gel Filtration Chromatography*

Analytical gel filtration studies were carried out on an AKTA FPLC system (GE Healthcare). Proteins at concentration of 10~20 μM in a volume of 100 μl were loaded on a Superose 12 10/300 GL column 20 (GE Healthcare) equilibrated with the buffer containing 50 mM Tris, pH 8.0, 100 mM NaCl, 1 mM DTT, and 1 mM EDTA. Protein elution was detected by absorbance at 280 nm.

GDI activity Assay

Measurements of AlF_4^- induced increase of intrinsic tryptophan fluorescence were performed on the PerkinElmer LS-55 spectrometer with excitation at 292 nm and emissio n at 3 4 2n m Purified $G\alpha_{i3}$ protein was diluted in 2-ml cuvettes to 200 nM in a pre-activation buffer (100 mM NaCl, 100 μM EDTA, 2 mM $MgCl_2$, 20 μM GDP, 20 mM Tris-HCl, pH 8.0) and incubated at 30 °C. At the time points 400 and 500 sec after $G\alpha_{i3}$ dilution, 2 mM NaF and 30 μM $AlCl_3$ (final concentrations) were added respectively to the reaction mixture, and fluorescence intensity changes as a function of time were recorded. The GDI activities of GL peptides were assayed by repeating the above procedure except that the reaction mixtures contained defined concentrations of specific peptides.

The measurements of GTPγS binding were also performed on PerkinElmer LS-55 spectrometer with excitation at 485 nm and

emission at 530 nm (slit widths each at 2.5 nm). BODIPY FL-GTPγS was diluted to 1 μM in buffer (20 mM Tris-HCl, pH 8.0, 1 mM EDTA and 10 mM $MgCl_2$) and equilibrated to 30 °C in 2-ml cuvettes. Purified $G\alpha_{i3}$ was diluted to 100 nM in the buffer (100 mM NaCl, 100 μM EDTA, 2 mM $MgCl_2$, 20 μM GDP, 20 mM Tris-HCl, pH 8.0) and pre-incubated with GL peptides (with different concentrations) at 30 °C for 10 min before the addition to the cuvette. Relative fluorescence levels were set to zero at the average fluorescence reading over the first 70 s, and $G\alpha_{i3}$/GL mixtures were added at the time point of 100 sec.

Crystallography

Crystals of the $G\alpha_{i1(3)}$ in complex with GL3/4 (diluted to 7.5 mg/ml in 50 mM Tris, pH 8.0, 100 mM NaCl, 1 mM EDTA, 1 mM DTT, 10 mM Mg^{2+}, 20 μM GDP buffer) were obtained by the hanging drop vapor diffusion method at 18 °C. The crystals were grown in buffer containing 0.5 M ammonium sulfate, 1.0 M lithium sulfate monohydrate, 0.1 M sodium citrate tribasic dehydrate, pH 5.6. Crystals were soaked in crystallization solution containing a higher concentration (1.5 M) of lithium sulfate for cryo-protection. All the diffraction data were collected at Shanghai Synchrontron Radiation Facility BL17U at wavelength of 0.9793 Å using a single crystal of each complex. The diffraction data were processed and scaled using HKL2000 (35). Molecular replacement was used to solve the structure of $G\alpha_{i1(3)}$/GL4(3) with the program Molrep (36). The crystal structure of RGS14/$G\alpha_{i1}$ complex (1KJY) was used as a search model by removing the RGS14 peptide. The initial model was rebuilt manually and then refined using REFMAC (37) and PHENIX (38) against the whole data set. Further manual model building and adjustment were completed using COOT (39). The final refinement statistics are summarized in Table I.

Results

Mapping the minimal $G\alpha_i$·GDP binding sequences in LGN GoLoco motifs

The C-terminal region of LGN contains four GoLoco motifs, each of which consists of a conserved 19-residue fragment followed by a stretch of variable amino acid residues with different lengths (Fig. 1A). We define the full-length GoLoco motif to be the conserved 19-residue plus all of the following C-terminal sequence before the start of the next GoLoco motif core. With this definition, each GL1, 2, 3 and 4 motif of LGN consists of 54, 51, 34 and 51 residues, respectively (Fig. 1A). Previous structural study of the $G\alpha_{i1}$/RGS14-GoLoco complex showed that the 16-residue sequence C-terminal to the GoLoco core motif make extensive contacts with $G\alpha_{i1}$ and thus are essential for the interaction between $G\alpha_{i1}$ and RGS14 (14). To understand the interaction between LGN and $G\alpha_i$, we set out to map the minimal $G\alpha_i$·GDP binding sequence of each LGN GL. We first used GST-fused LGN GL with different lengths to pull down purified $G\alpha_{i3}$·GDP in our binding assay. This assay showed that each GL containing only the 19-residue core displayed only a background level of binding to $G\alpha_{i3}$·GDP (Fig. 1B). Obvious binding of $G\alpha_{i3}$·GDP to GL1 and GL4 was observed by extending the conserved 19-residue GL core by 2 residues (Fig. 1B). Any one of LGN GLs with length equal to or longer than 25 residues displayed comparable bindings to their corresponding full-length motifs (Fig. 1B). We next measured the quantitative binding affinities of each of the four GLs to $G\alpha_{i3}$·GDP using isothermal titration calorimetry or fluorescence spectroscopy. Such quantitative binding assays revealed that the

four full-length GLs share similar affinities (K_D: 54 ~ 96 nM) in binding to $G\alpha_{i3}$·GDP (Fig. 1C). In agreement with the results derived from the pull-down binding assay, each LGN GL with a length of 25 residues has an essentially same binding affinity compared to the corresponding full-length motif (Fig. 1C), indicating that each of the 25-residue LGN GL contains the complete $G\alpha_i$·GDP binding sequence. This finding is in sharp contrast to the interaction between $G\alpha_i$·GDP and the RGS14 GoLoco motif, which requires a total length of 35 residues (14). Consistent with earlier studies (40), the LGN GLs bind to $G\alpha_{i3}$·GTPγS with a ~100-fold weaker affinity than to $G\alpha_{i3}$·GDP (data not shown).

$G\alpha_i$·GDP can simultaneously bind to all four LGN GLs

We next asked whether $G\alpha_i$·GDP can simultaneously bind to the multiple GLs of LGN. We first tested the interaction between $G\alpha_i$·GDP and the LGN GL34 tandem (aa 587-650), as the intervening sequence between the core sequences of GL3&4 are the shortest (15 residues to be exact, Fig. 1A). According to the structure of $G\alpha_{i1}$/RGS14 complex (14), two successive GL core sequences separated by a 15-residue linker cannot bind to two $G\alpha_i$ as the bound $G\alpha_i$ molecules would crash into each other. We examined the binding stoichiometry between LGN-GL34 and $G\alpha_{i3}$·GDP using analytical gel-filtration chromatography. Upon addition of 2 or 3 molar ratios of $G\alpha_{i3}$ to GL34, a peak corresponding to a $(G\alpha_{i3}\cdot GDP)_2$/GL34 complex was detected (Fig. 2A), indicating that the two GLs in GL34 can simultaneously bind to $G\alpha_{i3}$·GDP. To further substantiate that the elution peak at ~11.60 ml in Fig. 2A represents the 2:1 stoichiometric complex formed between $G\alpha_{i3}$·GDP and GL34, we used two GL34 mutants (L594E and I628E), in which either the $G\alpha_{i3}$·GDP binding site on GL3 (the L594E mutant) or on GL4 (the I628E mutant) was disrupted. On the gel-filtration column, the 1:2 mixtures of the two GL34 mutants with $G\alpha_{i3}$·GDP were eluted at a volume significantly larger than the wild type GL34 and a large portion of free $G\alpha_{i3}$·GDP was also detected (Fig. 2B), presumably that the GL34 mutants only formed 1:1 stoichiometric complex with $G\alpha_{i3}$·GDP. This result also confirms that the wild type GL34 can form a 1:2 stoichiometric complex with $G\alpha_{i3}$·GDP. Further lengthening of the linker between GL3 and GL4 by inserting ten flexible residues (five GS repeats, referred to as "GL34Ins5GS") did not alter the elution profile of its complex with $G\alpha_{i3}$·GDP (data not shown), indicating that the 15-residue intervening sequence between GL3 and GL4 is sufficiently long for two molecules of $G\alpha_{i3}$·GDP to bind simultaneously to GL34. Similarly, two molecules of $G\alpha_{i3}$·GDP are capable of binding to LGN-GL12 (aa 483-586) or GL23 (aa 537-620). (Fig. 2C&D). Additionally, three molecules of $G\alpha_{i3}$·GDP were found to bind simultaneously to GL123 (aa 483-620) or GL234 (aa 537-650) of LGN (Fig. 2E&F).

To characterize the binding stoichiometry more precisely, ITC analyses were performed. The titration profiles of $G\alpha_{i3}$·GDP to GL23 and GL34 can be well fitted with the 'one set of identical sites' model, yielding the overall stoichiometry of 1.9:1 and 1.8:1, respectively (Fig. 3A&B, Table II), consistent with the binding stoichiometry derived from the gel-filtration analyses. The apparent binding affinity of GL23 was similar with those of the individual GoLocos, while GL34 had a weaker binding affinity than that of GL3 or

GL4 (Table II, Fig. 1C). The titration profile of $G\alpha_{i3}$·GDP to the triple-GoLoco-containing protein GL234 was also fitted with the 'one set of binding sites' model, giving a weaker binding affinity of ~ 358 nM and the binding stoichiometry of 3.1:1 (Fig. 3C, Table II). The purified GL234 protein underwent slight degradation, which might affect the accuracy of the binding affinity measurement. The titration profile of $G\alpha_{i3}$·GDP to GL12, however, was best fitted with the model that assumes two sets of binding sites (Fig. 3D), yielding one strong site (K_D ~ 11 nM) and one weak site (K_D ~ 188 nM) (Table II). The ITC titration profile of $G\alpha_{i3}$·GDP to GL123 was also fitted with the 'two sets of binding sites' model, giving rise to two strong sites (K_D ~ 4 nM) and one weak site (K_D ~ 186 nM) (Fig. 3E, Table II). Similar atypical profiles of ITC titrations were also observed in the analyses of AGS3-GLs/$G\alpha_i$·GDP interaction (41). It is worth noting that these data analyses do not represent the complete description of the thermodynamics of the interactions between tandem LGN-GoLoco repeats and $G\alpha_{i3}$·GDP, in which inter-site cooperativity likely exists. Since the full-length GoLoco region of LGN, i.e. GL1234, suffers from severe degradation, we did not analyze the binding property of GL1234 directly. However, the ITC titration data, consistent with the gel-filtration analyses, strongly suggested that the full length LGN binds $G\alpha_{i3}$·GDP with a stoichimetry of 1:4. The four GoLoco motifs of LGN have intrinsically similar binding affinities to $G\alpha_{i3}$·GDP. To explore the molecular details of the binding, we proceeded to determine the crystal structure of $G\alpha_i$/LGN-GoLoco complex.

Overall crystal structures of GL3 and GL4 in complex with $G\alpha_i$·GDP

Extensive efforts have been put to screen various constructs of the four LGN GLs in complex with GDP-loaded $G\alpha_{i3}$ or $G\alpha_{i1}$, and we succeeded in obtaining well-diffracting crystals for synthetic GL4 (^{621}DEDFFSLILRSQAKRMDEQRVLLQR D^{645}) and GL3 (^{587}DEDFFDILVKCQGSRLDDQRCAPPS^{6} ^{11}) peptides in complex with $G\alpha_{i1/3}$·GDP. The $G\alpha_{i1}$/GL4, $G\alpha_{i3}$/GL4 and $G\alpha_{i3}$/GL3 complexes diffracted to 2.9, 3.5 and 3.6 Å resolutions, respectively (Table I). According to a previous structure-based protein design study, point mutations on $G\alpha_i$ (E116L, Q147L and E245L, respectively) can enhance its binding affinity to various GLs (15). We therefore constructed such three $G\alpha_{i3}$ mutants, hoping that the mutants might have higher affinities in binding to LGN GLs and thus yield better quality complex crystals. Opposite to our expectation, none of these mutants showed obviously enhanced binding to LGN GLs (data not shown). Nonetheless, the Q147L-$G\alpha_{i3}$ mutant/GL4 complex yielded better diffracting crystals (2.9 Å) than the wild type $G\alpha_{i3}$/GL4 complex.

The structure of $G\alpha_{i1(3)}$/GL4 and $G\alpha_{i3}$/GL3 were solved by molecular replacement using the $G\alpha_{i1}$/RGS14 structure as the search model (PDB ID: 1KJY) (14). The $G\alpha_i$·GDP structure is well defined, and 21~22 amino acids of the GL3 or GL4 peptide are ordered in the structures of complexes (Fig. 4A, B). The structures of $G\alpha_i$ in the $G\alpha_{i1(3)}$/GL4 and $G\alpha_{i3}$/GL3 complexes are highly similar to that in the $G\alpha_{i1}$/RGS14 complex (RMSD of 0.67 Å), except for the Switch II region, which is shifted further away from the LGN-GL peptides due to the presence of two bulky hydrophobic residues in the GL peptides (Fig. 5A&B). The GL peptides in the three complexes adopt highly similar structures

(Fig. 4C). The N-terminal 10 residues of each LGN GL peptide (aa 623-632 of GL4 and aa 589-598 of GL3), which corresponds to the first half of the conserved 19-residue GL core, forms an α-helix which occupies the cleft between the Switch II and α3 of $G\alpha_i$ (Fig. 4A). The following 8 residues of the GL core (aa633-640 of GL4 and aa599-606 of GL3) forms a "lid" in covering GDP. Only 3-4 residues C-terminal to the GL core (aa641-643 of GL4 and aa607-610 of GL3) were found to bind to the all-helical domain of $G\alpha_i$ (Fig. 4). The structures of the LGN GL peptides in complex with $G\alpha_i$ are entirely consistent with our biochemical data showing that extending of the conserved GL core at the C-terminal end by 3-4 residues is necessary and sufficient for LGN GLs to bind to $G\alpha_i$ (Figs. 1&2). The structures of the complexes also indicate that LGN GLs should function as GDIs by directly stabilizing the bound GDP as well as the interaction between the Ras-like domain and the all-helical domain of $G\alpha_i$ (Fig. 4A).

A general interaction mode revealed by the LGN GLs in complex with $G\alpha_i$

Although the structures of $G\alpha_i$ bound to the GLs of RGS14 and LGN are highly similar, the conformation of $G\alpha_i$-bound GLs of RGS14 and LGN are distinctly different (Fig. 5). First, a 16-residue fragment C-terminal to the conserved GL core of RGS14 is required for binding to $G\alpha_i$, and this 16-residue fragment forms ordered structure and has extensive interactions with the all-helical domain of $G\alpha_{i1}$ (14). In LGN-GL4/GL3, in contrast, only 3-4 residues C-terminal to the GL core are required for binding to $G\alpha_i$ (Fig. 4A). Second, the orientation of the variable C-terminal tail of the RGS14 GL peptide is opposite to that of the LGN GL peptides (Fig. 5A). In the LGN GL4/$G\alpha_i$ complex, the hydrophobic side chains of V641, L642 and L643 interact with V72 and Y69 from the αA helix of the $G\alpha_i$ all-helical domain, thus the C-terminal end of GL4 extends towards the N-terminal end of $G\alpha_i$ αA (Fig. 5C). Residue corresponding to V641 in the RGS14 peptide is G517 (Fig. 5D and Fig. 6A). The backbone carbonyl oxygen of G517 forms two hydrogen bonds with side chains of S75 and Q79 from $G\alpha_i$ αA. The unique backbone dihedral angles ($\phi = 78°$, $\psi = -171°$) of G517, which are not allowed by other amino acids, enable the C-terminal tail of the RGS14 GL peptide to take a sharp turn at this position and extend to the C-terminal end of $G\alpha_i$ αA (Fig. 5A&D). Sequence alignment of all known GLs from mammals reveals that only the GLs of RGS14 and RGS12 contain a Gly right after the conserved core motif, and the C-terminal residues of these two GLs share the identical sequence (Fig. 6A). The above structure-based amino acid sequence analysis suggests that the LGN GL/$G\alpha_i$ interactions observed in this study represent the general mode of the interactions between GoLoco proteins and $G\alpha_i$. RGS14 and RGS12, instead, may represent a special sub-class of GoLoco proteins in terms of $G\alpha_i$ binding.

The "double Arg-finger"-mediated GDP binding of LGN GLs

The structure of the $G\alpha_{i1}$/RGS14 GL complex shows that a highly conserved "D/E-Q-R" triad at the C-terminal end of the conserved GL core plays a critical role in binding to Mg^{2+}-GDP (14). Similar to the $G\alpha_{i1}$/RGS14 GL interaction, the side chain of R640 (R606) of GL4 (GL3) in the 'D/E-Q-R' triad, which is equivalent to R516 of RGS14, is inserted into the GDP binding pocket and binds to α-phosphate of

GDP (Fig. 6B). However, there is a distinct feature of GL4/GL3 in GDP binding with respect to RGS14 GL. Another highly conserved Arg five residues upstream of the Arg in the "D/E-Q-R" triad in LGN GL peptides (R635 in GL4 and R601 in GL3) binds to the α and β phosphates of GDP (Fig. 6B). In RGS14 GL, the residue corresponding to this second Arg is a Gly, and a Mg^{2+} ion was found to be necessary to stabilize the β phosphates of GDP (14). Therefore, different from RGS14, LGN GLs use two Arg residues instead of one to bind to and stabilize GDP. The structures of the LGN GLs in complex with $G\alpha_i$ further indicate that the LGN GLs can bind to GDP-bound $G\alpha_i$ independent of the presence of Mg^{2+}. This structure-based prediction is confirmed by direct binding experiment (data not shown). Sequence alignment analysis reveals that, except for RGS14 GL, the rest of GLs all contain a "R/K-X-D/E-D/E-Q-R", GDP binding sequence (Fig. 6A), and we refer this sequence as the "double Arg-finger". This sequence analysis further supports that the LGN GL/$G\alpha_i$ interaction represents the general mode of GL-mediated binding to Gα.

The double-arginine fingers are critical to the GDI activities of LGN-GLs

To confirm the functional importance of the two Arg in the double-arginine finger in LGN GLs, we performed point mutations of the two arginines, and tested the $G\alpha_i$·GDP binding affinities and GDI activities of these mutants. Single substitution mutations (R635G, R635A, and R640A) caused ~50-fold decrease in GL4's binding to $G\alpha_i$·GDP, and the double mutation (R635,640A) led to ~500-fold $G\alpha_i$·GDP binding affinity decrease (Fig. 6C). Similar results were also obtained from the other LGN GLs, indicating that the two conserved arginine fingers are critical for binding of $G\alpha_i$·GDP to LGN-GLs. This finding is in contrast to the RGS14 GL, in which the substitution of the Arg in the finger with Ala or Leu did not decrease the binding affinity of RGS14 to $G\alpha_{i1}$·GDP (14). Careful examination of the crystal structures of $G\alpha_i$ in complex with LGN GL peptides revealed that the side chains of the two Arg residues also form hydrogen bonds with V179 and T181 from $G\alpha_i$ (Fig. 6B). In contrast, the side chain of R516 in RGS14 GL interacts exclusively with GDP (14).

The GDI activities of LGN GLs were evaluated by AlF_4^- induced increase of intrinsic tryptophan fluorescence of $G\alpha_i$ and by direct binding of BODIPY-GTPγS to $G\alpha_i$. In agreement with the previous studies (40), the four GLs exhibited similar GDI activities (data not shown). Moreover, comparison of the GDI activities of GL peptides with different lengths showed that the 25-residue minimal $G\alpha_i$-binding GL fragments shown in Fig. 1 are also sufficient for their GDI activities (data not shown). Further quantification of the GDI activities using the association rate of BODIPY-GTPγS binding revealed IC_{50} values of a few μM for LGN GLs, which is slightly weaker than that of RGS14 GL (data not shown). At a saturated concentration of GL peptide (GL: 200 μM, $G\alpha_{i3}$: 0.2 μM), the wild type LGN-GL4 showed a complete inhibition of GDP dissociation from $G\alpha_{i3}$ (Fig. 6D). The R635G-GL4 or the R635A-GL4 displayed obviously weakened GDI activities, whereas the R640A-GL4 and R635,640A-GL4 had essentially no detectable GDI activity (Fig. 6D). Substitution of the first Arg (R601) in the double-arginine finger of GL3 with Ala or Gly also diminished its GDI activity (data not shown). Thus, we conclude that both

Arg in the double-arginine finger of LGN GoLoco motifs are important for their GDI activity.

Discussion

Both the binding to GDP-loaded Gα subunits and the GDI activity of GL require residues beyond the 19-residue conserved core sequence (14,41). Since the C-terminal flanking sequences of GLs are highly diverse among GoLoco proteins (7), it has been hypothesized that the variable C-terminal tail sequences of GLs are the specificity determinants governing GL/Gα interactions. In the present study, we demonstrate that only a few residues (3-4 aa) C-terminal to the conserved GL core are required for LGN GLs to bind to and to inhibit GDP dissociation of $G\alpha_i$·GDP, a finding which is in sharp contrast to that of RGS14 GL. Sequence alignment analysis suggests that the conformation of the GL peptide in the $G\alpha_{i1}$/RGS14 structure is likely a unique example of GL/Gα interaction. The LGN GL/$G\alpha_i$ interaction described in the current study instead is likely a general binding mode between GLs and Gα. The structures of LGN GLs in complex with $G\alpha_i$·GDP also suggest that the short variable C-terminal sequences of LGN GLs are unlikely to determine their binding specificity to Gα subunits. Consistently, previous studies have shown that LGN GLs bind to all three forms of GDP-loaded $G\alpha_i$ (i1, i2, i3). As for the $G\alpha_o$·GDP binding, discrepancies exist in the literatures. An early study by McCudden et al. reported that LGN GLs selectively bind to $G\alpha_i$·GDP, but not to $G\alpha_o$·GDP or $G\alpha_s$·GDP (40). Recently, Kopein et al. found that LGN, as well as its *Drosophila* homolog Pins, can bind robustly to both GDP-loaded $G\alpha_o$ and $G\alpha_i$(42).

We have demonstrated in this study that every one of the four LGN GLs can bind to $G\alpha_i$·GDP with high affinity. Additionally, although the LGN GL peptides are much shorter than their counterpart from RGS14, LGN GLs also act as potent GDIs. The structures of the LGN GL3 and GL4 in complex with $G\alpha_i$ suggest that both the double-arginine finger and the short variable tail of the GL peptides are important for their GDI activities. The di-arginine finger makes extensive salt bridges with the phosphates of GDP, and the GDP in return makes contacts with both the Ras-like and all-helical domains of $G\alpha_i$. The variable C-terminal tail of the GL peptides further interacts with the all-helical domain of $G\alpha_i$. Thus, in addition to stabilize GDP bound to $G\alpha_i$, the binding of GL peptide further promotes the closed conformation of $G\alpha_i$ (i.e. by restricting the opening of the all-helical domain and subsequent dissociation of GDP from $G\alpha_i$, Fig. 7).

The characteristic multiple GLs in LGN and its *Drosophila* homolog Pins have been implicated to play a role in regulating their intra-molecular interactions between TPR repeats and GLs in response to the binding of $G\alpha_i$·GDP and NuMA/Mud (34,43). Besides this, the multiple GLs in LGN (Pins) also function as a scaffold in regulating the localization of related protein complexes and organizing signaling pathways mediating spindle orientations. The detailed characterizations of interactions between LGN-GLs and $G\alpha_i$·GDP in this work demonstrate that in its open state the four LGN GLs have equal capacity to bind to $G\alpha_i$·GDP (Fig. 6E). In another word, the stoichiometry of LGN/$G\alpha_i$·GDP complex *in vivo* likely depends on the concentration of $G\alpha_i$·GDP, which in turn regulates the cortical localization of LGN-bound proteins, such as NuMA. Recently, it was found that the extrinsic GPCR Tre1 signaling determines

the orientation of cortical polarity in the asymmetric cell division of *Drosophila* neuroblast (44). Tre1 was shown to activate $G\alpha_o$, and the GTP form $G\alpha_o$ can specifically associate with the first GL of Pins (44). Thus, the presence of multiple GLs allows Pins to function as a scaffold to simultaneously engage $G\alpha_o$- and $G\alpha_i$-mediated signaling events during asymmetric cell division.

References

1. Malbon, C. C. (2005) *Nat Rev Mol Cell Biol* **6**, 689-701
2. Sprang, S. R. (1997) *Annu Rev Biochem* **66**, 639-678
3. Gilman, A. G. (1987) *Annu Rev Biochem* **56**, 615-649
4. Sunahara, R. K., Dessauer, C. W., and Gilman, A. G. (1996) *Annu Rev Pharmacol Toxicol* **36**, 461-480
5. Singer, W. D., Brown, H. A., and Sternweis, P. C. (1997) *Annu Rev Biochem* **66**, 475-509
6. Kozasa, T., Jiang, X. J., Hart, M. J., Sternweis, P. M., Singer, W. D., Gilman, A. G., Bollag, G., and Sternweis, P. C. (1998) *Science* **280**, 2109-2111
7. Willard, F. S., Kimple, R. J., and Siderovski, D. P. (2004) *Annu Rev Biochem* **73**, 925-951
8. Siderovski, D. P., Diverse-Pierluissi, M., and De Vries, L. (1999) *Trends Biochem Sci* **24**, 340-341
9. Bernard, M. L., Peterson, Y. K., Chung, P., Jourdan, J., and Lanier, S. M. (2001) *J Biol Chem* **276**, 1585-1593
10. Kimple, R. J., De Vries, L., Tronchere, H., Behe, C. I., Morris, R. A., Gist Farquhar, M., and Siderovski, D. P. (2001) *J Biol Chem* **276**, 29275-29281
11. Natochin, M., Gasimov, K. G., and Artemyev, N. O. (2001) *Biochemistry* **40**, 5322-5328
12. Granderath, S., Stollewerk, A., Greig, S., Goodman, C. S., O'Kane, C. J., and Klambt, C. (1999) *Development* **126**, 1781-1791
13. Ponting, C. P. (1999) *J Mol Med (Berl)* **77**, 695-698
14. Kimple, R. J., Kimple, M. E., Betts, L., Sondek, J., and Siderovski, D. P. (2002) *Nature* **416**, 878-881
15. Bosch, D. E., Kimple, A. J., Sammond, D. W., Muller, R. E., Miley, M. J., Machius, M., Kuhlman, B., Willard, F. S., and Siderovski, D. P. (2011) *J Biol Chem* **286**, 3351-3358
16. Sammond, D. W., Eletr, Z. M., Purbeck, C., Kimple, R. J., Siderovski, D. P., and Kuhlman, B. (2007) *J Mol Biol* **371**, 1392-1404
17. Sammond, D. W., Bosch, D. E., Butterfoss, G. L., Purbeck, C., Machius, M., Siderovski, D. P., and Kuhlman, B. (2011) *J Am Chem Soc* **133**, 4190-4192
18. Bosch, D. E., Willard, F. S., Ramanujam, R., Kimple, A. J., Willard, M. D., Naqvi, N. I., and Siderovski, D. P. (2012) *PLoS Pathog* **8**, e1002553
19. Du, Q., Stukenberg, P. T., and Macara, I. G. (2001) *Nat Cell Biol* **3**, 1069-1075
20. Zhu, J., Wen, W., Zheng, Z., Shang, Y., Wei, Z., Xiao, Z., Pan, Z., Du, Q., Wang, W., and Zhang, M. (2011) *Mol. Cell* **43**, 418-431
21. Du, Q., Taylor, L., Compton, D. A., and Macara, I. G. (2002) *Curr Biol* **12**, 1928-1933
22. Du, Q., and Macara, I. G. (2004) *Cell* **119**, 503-516
23. Siller, K. H., Cabernard, C., and Doe, C. Q. (2006) *Nat Cell Biol* **8**, 594-600
24. Izumi, Y., Ohta, N., Hisata, K., Raabe, T., and Matsuzaki, F. (2006) *Nat Cell Biol* **8**, 586-593

25. Bowman, S. K., Neumuller, R. A., Novatchkova, M., Du, Q., and Knoblich, J. A. (2006) *Dev Cell* **10**, 731-742
26. Colombo, K., Grill, S. W., Kimple, R. J., Willard, F. S., Siderovski, D. P., and Gonczy, P. (2003) *Science* **300**, 1957-1961
27. Gotta, M., Dong, Y., Peterson, Y. K., Lanier, S. M., and Ahringer, J. (2003) *Curr Biol* **13**, 1029-1037
28. Srinivasan, D. G., Fisk, R. M., Xu, H., and van den Heuvel, S. (2003) *Genes Dev* **17**, 1225-1239
29. Bellaiche, Y., Radovic, A., Woods, D. F., Hough, C. D., Parmentier, M. L., O'Kane, C. J., Bryant, P. J., and Schweisguth, F. (2001) *Cell* **106**, 355-366
30. Sans, N., Wang, P. Y., Du, Q., Petralia, R. S., Wang, Y. X., Nakka, S., Blumer, J. B., Macara, I. G., and Wenthold, R. J. (2005) *Nat. Cell Biol.* **7**, 1179-1190
31. Zhu, J., Shang, Y., Xia, C., Wang, W., Wen, W., and Zhang, M. (2011) *EMBO J.* **30**, 4986-4997
32. Yu, F., Kuo, C. T., and Jan, Y. N. (2006) *Neuron* **51**, 13-20
33. Kaushik, R., Yu, F. W., Chia, W., Yang, X. H., and Bahri, S. (2003) *Mol Biol Cell* **14**, 3144-3155
34. Nipper, R. W., Siller, K. H., Smith, N. R., Doe, C. Q., and Prehoda, K. E. (2007) *Proc Natl Acad Sci U S A* **104**, 14306-14311
35. Otwinowski, Z., and Minor, W. (1997) *Macromolecular Crystallography, Pt A* **276**, 307-326
36. Vagin, A., and Teplyakov, A. (1997) *J. Applied Crystallogr.* **30**, 1022-1025
37. Murshudov, G. N., Vagin, A. A., and Dodson, E. J. (1997) *Acta Crystallogr D* **53**, 240-255
38. Adams, P. D., Afonine, P. V., Bunkoczi, G., Chen, V. B., Davis, I. W., Echols, N., Headd, J. J., Hung, L. W., Kapral, G. J., Grosse-Kunstleve, R. W., McCoy, A. J., Moriarty, N. W., Oeffner, R., Read, R. J., Richardson, D. C., Richardson, J. S., Terwilliger, T. C., and Zwart, P. H. (2010) *Acta Crystallogr. D Biol. Crystallogr.* **66**, 213-221
39. Emsley, P., and Cowtan, K. (2004) *Acta Crystallogr D* **60**, 2126-2132
40. McCudden, C. R., Willard, F. S., Kimple, R. J., Johnston, C. A., Hains, M. D., Jones, M. B., and Siderovski, D. P. (2005) *Biochimica Et Biophysica Acta-Molecular Cell Research* **1745**, 254-264
41. Adhikari, A., and Sprang, S. R. (2003) *J Biol Chem* **278**, 51825-51832
42. Kopein, D., and Katanaev, V. L. (2009) *Mol Biol Cell* **20**, 3865-3877
43. Smith, N. R., and Prehoda, K. E. (2011) *Mol. Cell* **43**, 540-549
44. Yoshiura, S., Ohta, N., and Matsuzaki, F. (2011) *Dev. Cell* **22**, 79-91
45. Chen, V. B., Arendall, W. B., 3rd, Headd, J. J., Keedy, D. A., Immormino, R. M., Kapral, G. J., Murray, L. W., Richardson, J. S., and Richardson, D. C. (2010) *Acta Crystallogr. D Biol. Crystallogr.* **66**, 12-21

FOOTNOTES

*We thank the Shanghai Synchrotron Radiation Facility (SSRF) BL17U for X-ray beam time. This work was supported by National Major Basic Research Program of China (2009CB918600, 2011CB808505), National Science Foundation of China (20973040, 31070642), Science & Technology Commission of Shanghai Municipality (08DZ2270500), and by grants (663808, 664009, 660709, 663610, 663811, HKUST6/CRF/10, and

SEG_HKUST06) from the Research Grants Council of Hong Kong to MZ. MZ is a Senior Fellow of the Institute for Advanced Study, HKUST.

The atomic coordinates and structure factors (code 4G5O, 4G5Q, 4G5R, and 4G5S) have been deposited in the Protein Data Bank, Research Collaboratory for Structural Bioinformatics, Rutgers University, New Brunswick, NJ(http://www.rcsb.org/).

FIGURE LEGENDS

Fig. 1. Characterization of the bindings between $G\alpha_i$·GDP and the four LGN GLs. (**A**) Schematic diagram of the domain organization of LGN. "DBM" denotes the DLG-binding domain of LGN. (**B**) GST-pull down assay of the bindings between LGN GLs with variable lengths (indicated by the number at the top of each GL) with $G\alpha_{i3}$·GDP. (**C**) ITC and fluorescence-based (denoted with stars) measurements of the binding affinities of $G\alpha_{i3}$·GDP with LGN GLs of different lengths.

Fig. 2. $G\alpha_i$·GDP binding to multiple GL containing fragments of LGN analyzed by analytical gel-filtration chromatography. (**A**) The bindings of LGN-GL34 to different molar ratios of $G\alpha_{i3}$·GDP. (**B**) The bindings of LGN-GL34(L594E) and LGN-GL34(I628E) to $G\alpha_{i3}$·GDP. (**C**) The bindings of LGN-GL12 to $G\alpha_{i3}$·GDP. (**D**) The bindings of LGN-GL23 to $G\alpha_{i3}$·GDP. (**E**) The bindings of LGN-GL123 to $G\alpha_{i3}$·GDP. (**F**) The bindings of LGN-GL234 to $G\alpha_{i3}$·GDP.

Fig. 3. ITC analyses of the bindings of tandem GoLoco motifs to $G\alpha_{i3}$·GDP. ITC measurements of bindings of $G\alpha_{i3}$·GDP to LGN-GL23 (**A**), LGN-GL34 (**B**), LGN-GL24 (**C**), LGN-GL12 (**D**) and LGN-GL13 (**E**). The titration data were fitted with the "one set of binding sites" or "two sets of binding sites" models. The derived thermodynamic parameters are shown in **Table II**.

Fig. 4. Crystal structures of $G\alpha_{i3}$ in complex with GL4 and GL3, respectively. (**A**) Ribbon diagram showing the crystal structure of LGN-GL4 in complex with $G\alpha_{i1}$·GDP. GDP is shown in the ball-and-stick model. All-helical domain and Ras-like domain of $G\alpha_{i1}$ is shown in wheat and light grey, respectively. The three switches are shown in violet, and the GL4 peptide is shown in cyan. (**B**) The F_o-F_c density map of GL4 peptide are shown in green and contoured at 3.0 σ. (**C**) Comparison of the structures of the $G\alpha_{i1}$/GL4, $G\alpha_{i3}$/GL4 and $G\alpha_{i3}$/GL3 complexes by superimposing the backbone atoms in the three structures. $G\alpha_{i1}$ is shown the same as in panel A, while $G\alpha_{i3}$ in complex with GL3 (RMSD of 0.76 Å) and GL4 (RMSD of 0.51 Å) are not shown. GL3 peptide is shown in blue and GL4 peptides bound to $G\alpha_{i1}$ and $G\alpha_{i3}$ are shown in red and green, respectively.

Fig. 5. Comparison of the crystal structures of $G\alpha_{i1}$/GL4 and $G\alpha_{i1}$/RGS14 complexes. (**A**) Comparison of the crystal structure of $G\alpha_{i1}$/GL4 (cyan) with that of $G\alpha_{i1}$/RGS14 (green). The all-helical domain and Ras-like domain of $G\alpha_{i1}$ are colored wheat and light grey, respectively. The Switch I, II and III regions of $G\alpha_{i1}$ in complex with LGN-GL4 and with RGS14 are highlighted with violet and light blue, respectively. (**B**) Comparison of the structural details of the α-helical region of LGN-GL4 and RGS14-GL, showing that the larger hydrophobic side chains of LGN-GL4 result in the shift of the Switch II of $G\alpha_{i1}$. (**C**) Structure details of the C-terminus of LGN-GL4, showing that two backbone hydrogen bonds stabilize the C-terminal conformation. (**D**) Structure details of the sharp turn at G517 of RGS14 peptide. Hydrogen bonds formed between RGS14 and $G\alpha_{i1}$ are shown with dashed lines.

Fig. 6. The double arginine fingers of the LGN GLs play a crucial role in GDP

coordination and GDI activity. (**A**) Sequence alignment of the GLs in mammalian GoLoco proteins. Absolutely and highly conserved residues are highlighted in red and yellow respectively. The residue right behind D/E-Q-R which determines the C-terminal direction is highlighted with blue triangle. The residues involved in the interactions with $G\alpha_i$ are labeled with a red star on the top. The di-arginine fingers are highlighted with black boxes. (**B**) Structural details of the GDP binding pocket in the $G\alpha_{i1}$/GL4 complex and $G\alpha_{i1}$/RGS14 complex. Polar interactions are shown with dashed lines. Distance of polar interaction is shown in magenta number (Å). The color scheme is the same as in Fig. 4A. (**C**) Binding affinities of the GL4 mutants with single or double substitutions of its two arginine residues to $G\alpha_{i3}$·GDP derived from fluorescence-based assays. (**D**) GDI activities of the wild type and mutant GL4 peptides measured with AlF_4^- induced increase of intrinsic tryptophan fluorescence. (**E**) Structural model of the LGN/$G\alpha_i$·GDP complex. TPR domain, the TPR-binding NuMA peptide and the GLs responsible for $G\alpha_i$·GDP binding are shown in blue, red and cyan respectively.

Figure 7 Comparison of $G\alpha_{i1}$/GL4 structure with the structure of the fully activated Gα conformation derived from the β_2-AR-Gαβγ structure. The all helical domain, Ras-like domain and three switches of GPCR bound $G\alpha_s$ are shown in light blue, pink and yellow, respectively. Part of the GPCR (β_2-AR**)** is shown in orange. The coloring of the $G\alpha_{i1}$/GL4 complex is the same as in Fig. 4A.

Table I Statistics of X-ray Crystallographic Data Collection and Model refinement

Data Sets	**Gα_{i3}^{QtoL}_GL4**	**Gα_{i1}_GL4**	**Gα_{i3}_GL4**	**Gα_{i3}_GL3**
Space Group	$P6_122$	$P6_122$	$P6_122$	$P6_122$
Unit cell (Å)	a=207.3 , c=236.6	a=207.4, c=236.7	a=209.6, c=237.2	a=209.7, c=235.5
No. of unique reflections	66825	66971	39388	35265
Resolution limit (Å)	50.00-2.90 (2.95-2.90)	50.00-2.90 (2.95-2.90)	50.00-3.50 (3.56-3.50)	50.00-3.60 (3.66-3.60)
Redundancy	10.8 (11.2)	9.4 (9.7)	4.4 (4.5)	9.2 (9.4)
Completeness (%)	100 (100)	100 (100)	98.8 (99.9)	99.7 (100)
I/σ_I	27.5 (3.6)	25.1 (3.3)	14.7 (1.8)	37.6 (5.8)
R_{merge} (%)	9.8 (76.2)	9.6 (73.5)	11.0 (75.7)	7.3 (39.6)
Structure refinement				
Resolution range (Å)	43.04-2.90 (3.00-2.90)	47.69-2.90 (3.00-2.90)	49.65-3.50 (3.61-3.48)	39.63-3.62 (3.75-3.62)
R_{cryst}/R_{free} (%)	22.0/25.0 (32.6/42.4)	22.0/24.5 (31.9/36.1)	22.6/26.1 (30.1/35.8)	22.8/25.3 (27.7/31.0)
Rmsd bonds (Å) / angle(°)	0.010/1.36	0.010/1.41	0.011/1.63	0.009/1.26
Average B factor ($Å^2$)	67.90	66.50	106.40	123.50
No. of atoms				
Protein atoms	10907	10921	10601	10141
Water molecules	12	35	0	0
Ligands	25	25	11	11
No. of reflections				
Working set	63256 (6246)	63457 (6234)	37222 (3584)	33318(3272)
Test set	3375(313)	3385 (343)	1963 (195)	1754(151)
Ramachandran plot				
Favored (%)	95.5	95.8	92.2	90.1
Allowed (%)	4.5	4.2	7.4	8.2
Outliers (%)	0	0	0.4	1.7

Numbers in parentheses represent the value for the highest resolution shell.

a. $R_{merge} = \Sigma |I_i - \langle I \rangle| / \Sigma I_i$, where I_i is the intensity of measured reflection and $\langle I \rangle$ is the mean intensity of all symmetry-related reflections.

b. $R_{cryst}=\Sigma||F_{calc}| - |F_{obs}||/\Sigma F_{obs}$, where F_{obs} and F_{calc} are observed and calculated structure factors. $R_{free}= \Sigma_T||F_{calc}| - |F_{obs}||/\Sigma F_{obs}$, where T is a test data set of about 5% of the total unique reflections randomly chosen and set aside prior to refinement.

c. B factors and Ramachandran plot statistics are calculated using MOLPROBITY(45).

Table II. Thermodynamic parameters of the bindings of LGN GoLoco motifs to $G\alpha_{i3}$·GDP determined by ITC titration

	N	K_D	ΔH	ΔS	ΔG
		nM	*kcal mol*$^{-1}$	*cal mol*$^{-1}$ *K*$^{-1}$	*kcal mol*$^{-1}$
GL12					
Site 1	0.97	11.27	-16.69	-18.7	-11.12
Site 2	0.89	188.32	-22.80	-44.4	-9.57
GL123					
Site 1	1.63	4.69	-12.55	-3.97	-11.37
Site 2	1.0	186.22	-15.46	-21.0	-9.20
GL23	1.86	87.72	-17.05	-24.0	-9.90
GL34	1.81	173.61	-20.97	-37.2	-9.88
GL234	3.08	358.42	-5.12	11.9	-8.67

The titration data of GL12 and GL123 were fitted with the 'two sets of binding sites' model, while the other data were fitted with the 'one set of binding sites' model. N denotes the number of binding sites in each model.

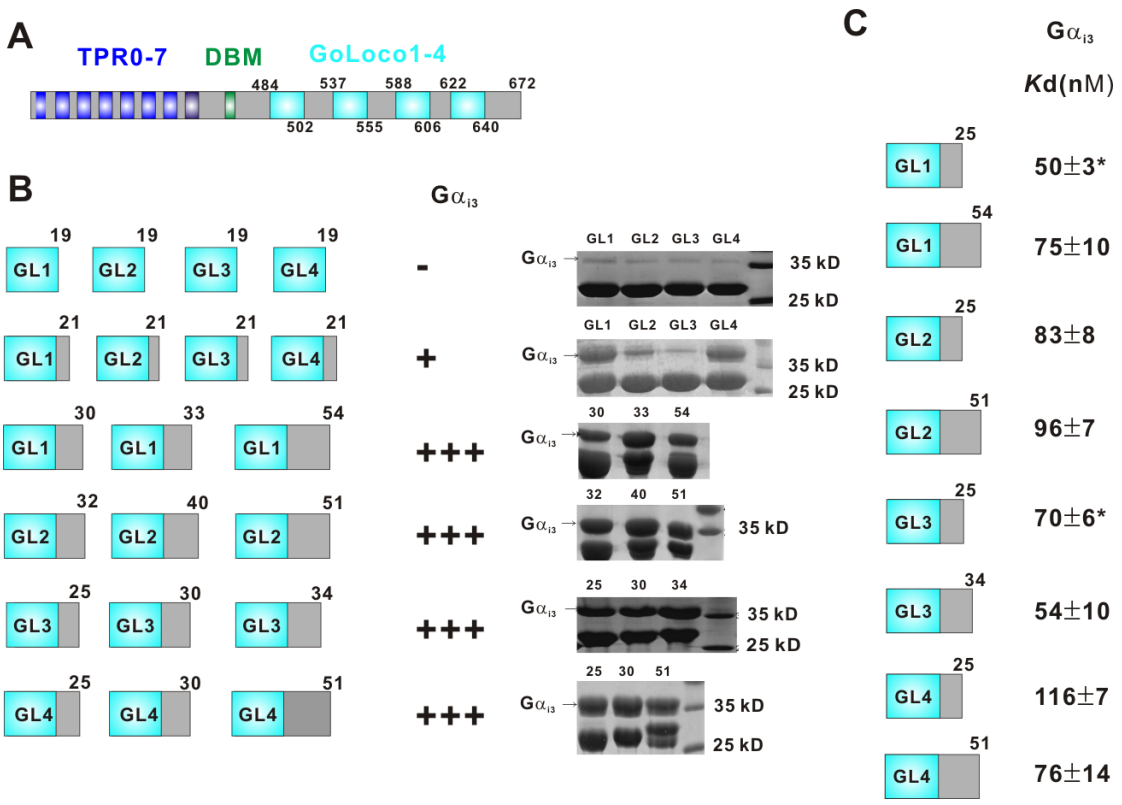
A
TPR0-7
DBM
GoLoco1-4
484
537
588
622
672
502
555
606
640
B
Gαi3
19
19
19
19
GL1
GL2
GL3
GL4
-
21
21
21
21
+
30
33
54
+++
32
40
51
+++
25
30
34
+++
25
30
51
+++
GL1 GL2 GL3 GL4
35 kD
25 kD
30 33 54
32 40 51
25 30 34
25 30 51
C
Gαi3
Kd(nM)
25
50±3*
54
75±10
25
83±8
51
96±7
25
70±6*
34
54±10
25
116±7
51
76±14

Figure 1

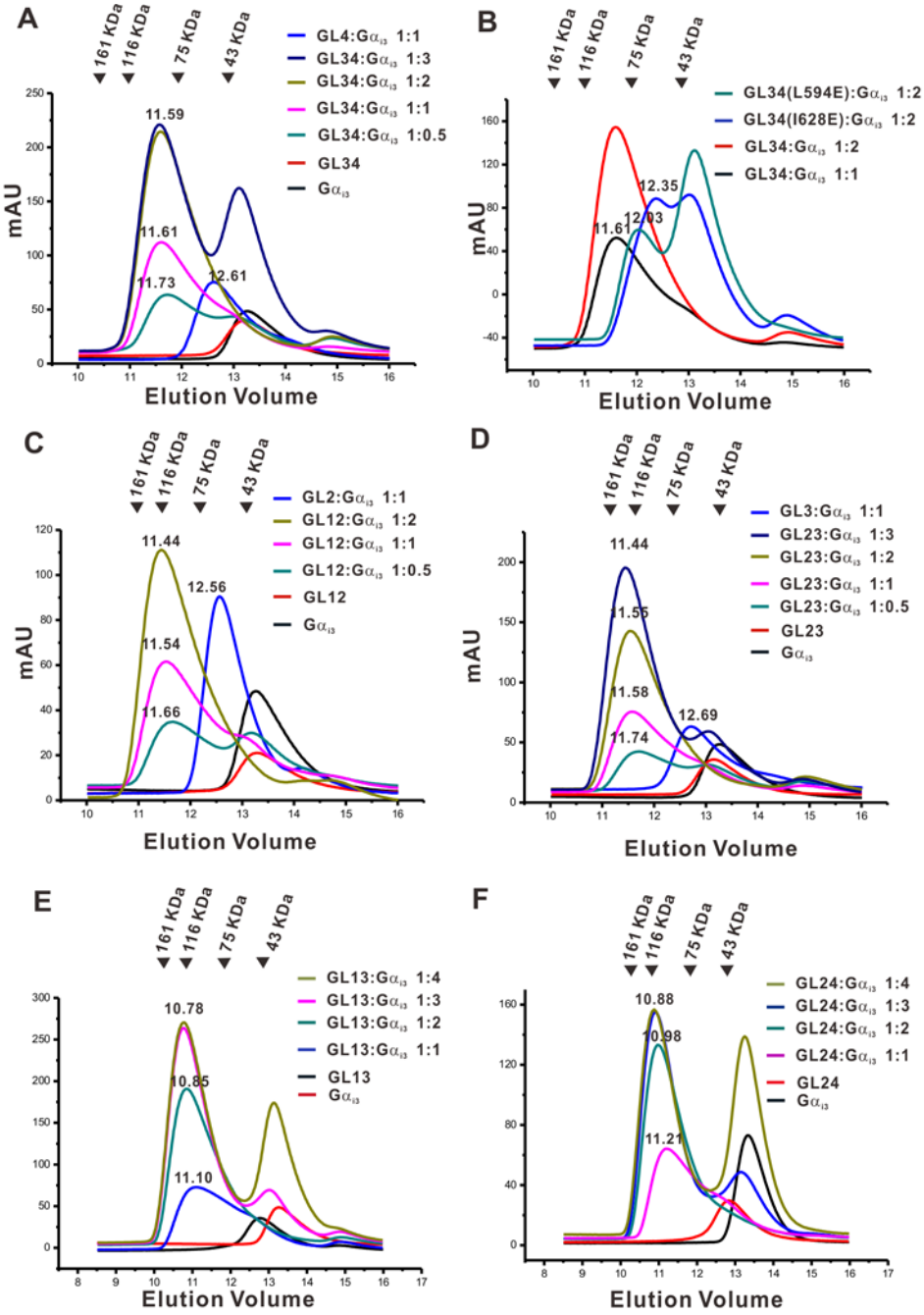
A
161 KDa
116 KDa
75 KDa
43 KDa
GL4:Gα13 1:1
GL34:Gα13 1:3
GL34:Gα13 1:2
GL34:Gα13 1:1
GL34:Gα13 1:0.5
GL34
Gα13
11.59
11.61
11.73
12.61
mAU
Elution Volume
B
161 KDa
116 KDa
75 KDa
43 KDa
GL34(L594E):Gα13 1:2
GL34(I628E):Gα13 1:2
GL34:Gα13 1:2
GL34:Gα13 1:1
12.35
12.03
11.61
mAU
Elution Volume
C
161 KDa
116 KDa
75 KDa
43 KDa
GL2:Gα13 1:1
GL12:Gα13 1:2
GL12:Gα13 1:1
GL12:Gα13 1:0.5
GL12
Gα13
11.44
12.56
11.54
11.66
mAU
Elution Volume
D
161 KDa
116 KDa
75 KDa
43 KDa
GL3:Gα13 1:1
GL23:Gα13 1:3
GL23:Gα13 1:2
GL23:Gα13 1:1
GL23:Gα13 1:0.5
GL23
Gα13
11.44
11.55
11.58
12.69
11.74
mAU
Elution Volume
E
161 KDa
116 KDa
75 KDa
43 KDa
GL13:Gα13 1:4
GL13:Gα13 1:3
GL13:Gα13 1:2
GL13:Gα13 1:1
GL13
Gα13
10.78
10.85
11.10
Elution Volume
F
161 KDa
116 KDa
75 KDa
43 KDa
GL24:Gα13 1:4
GL24:Gα13 1:3
GL24:Gα13 1:2
GL24:Gα13 1:1
GL24
Gα13
10.88
10.98
11.21
Elution Volume

Figure 2

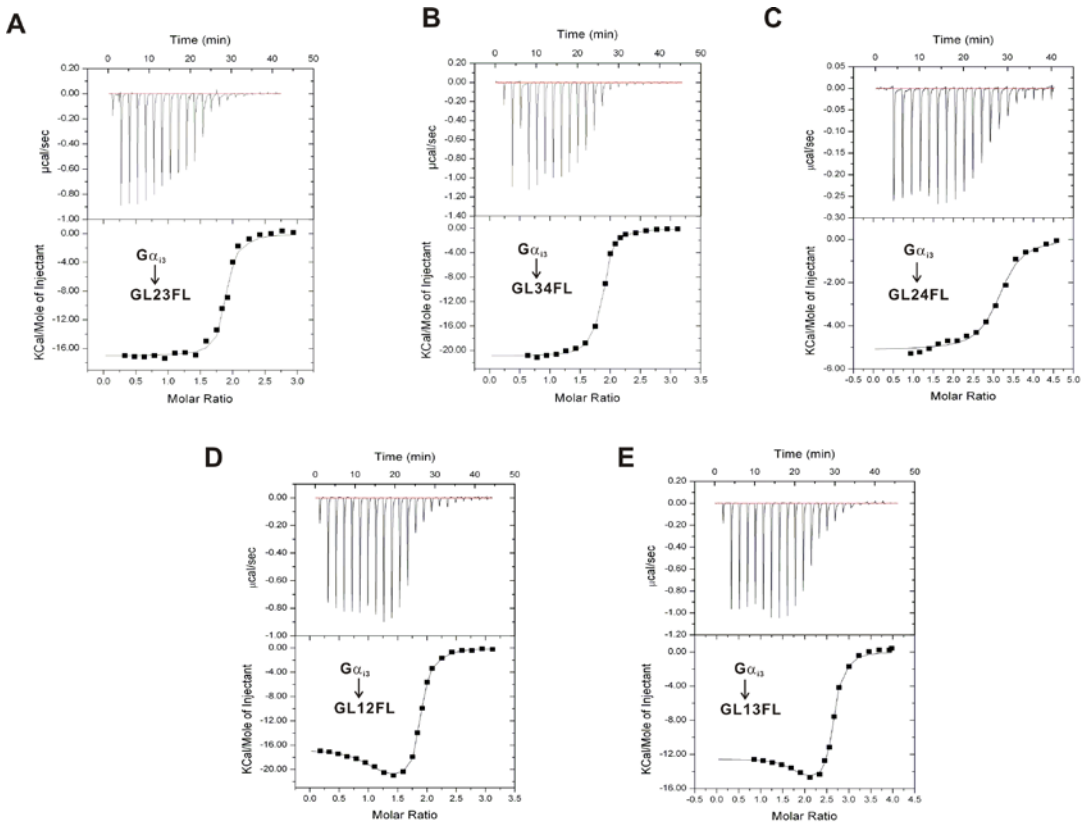
A
Time (min)
µcal/sec
KCal/Mole of Injectant
Gα13
GL23FL
Molar Ratio
B
Time (min)
µcal/sec
KCal/Mole of Injectant
Gα13
GL34FL
Molar Ratio
C
Time (min)
µcal/sec
KCal/Mole of Injectant
Gα13
GL24FL
Molar Ratio
D
Time (min)
µcal/sec
KCal/Mole of Injectant
Gα13
GL12FL
Molar Ratio
E
Time (min)
µcal/sec
KCal/Mole of Injectant
Gα13
GL13FL
Molar Ratio

Figure 3

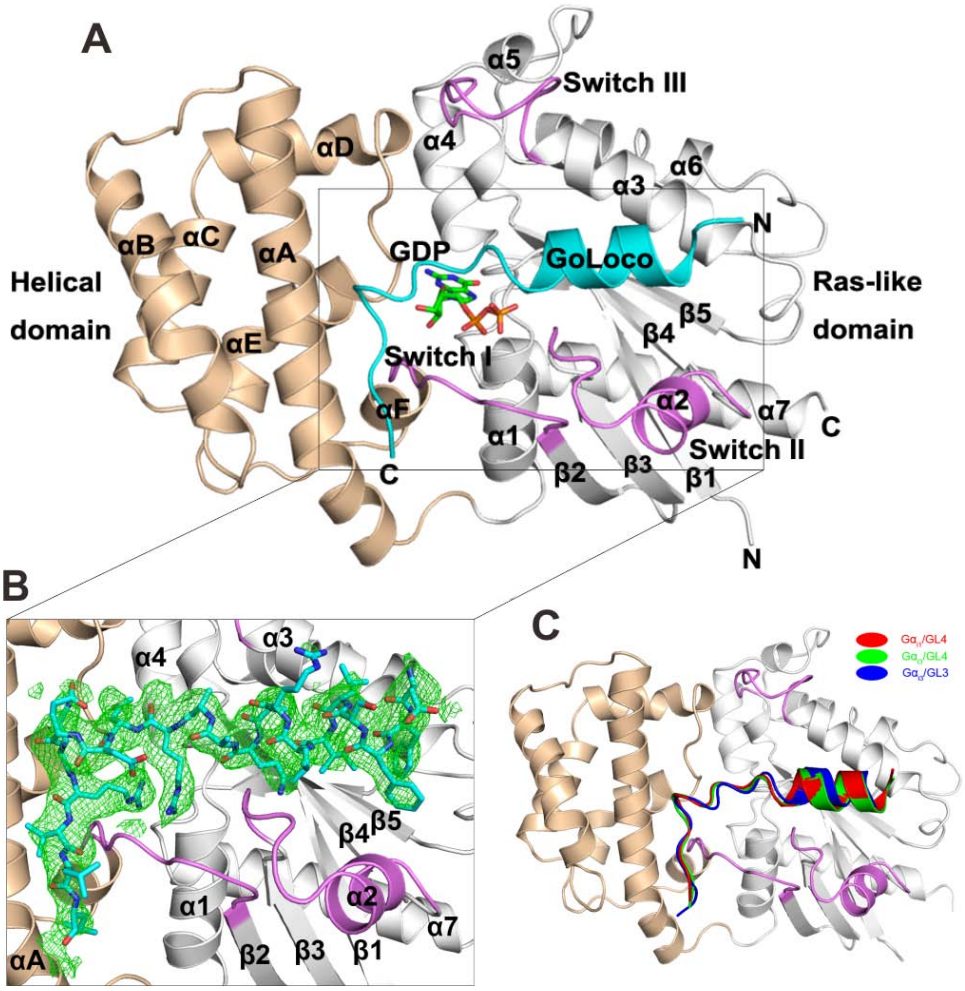
A
α5
Switch III
αD
α4
α6
α3
N
αB
αC
αA
GDP
GoLoco
Helical
domain
Ras-like
domain
β5
β4
αE
Switch I
αF
α2
α7
C
α1
Switch II
C
β2
β3
β1
N
B
α3
α4
β4
β5
α1
α2
α7
αA
β2
β3
β1
C
Gαi/GL4
Gαi/GL4
Gαi/GL3

Figure 4

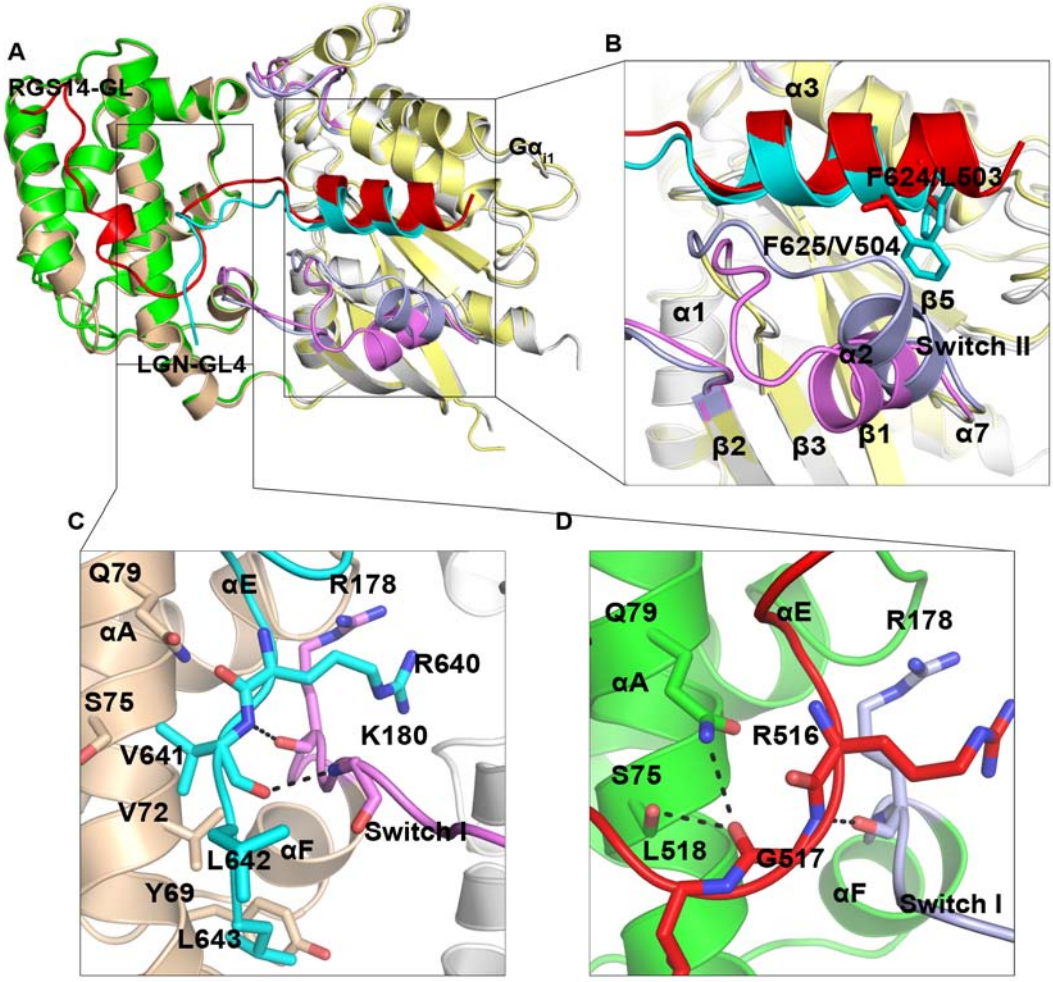
A
RGS14-GL
LGN-GL4
Gαi1
B
α3
F624/L503
F625/V504
α1
β5
α2
Switch II
β2
β3
β1
α7
C
Q79
αE
R178
αA
R640
S75
K180
V641
V72
Switch I
L642
αF
Y69
L643
D
Q79
αE
R178
αA
R516
S75
L518
G517
αF
Switch I

Figure 5

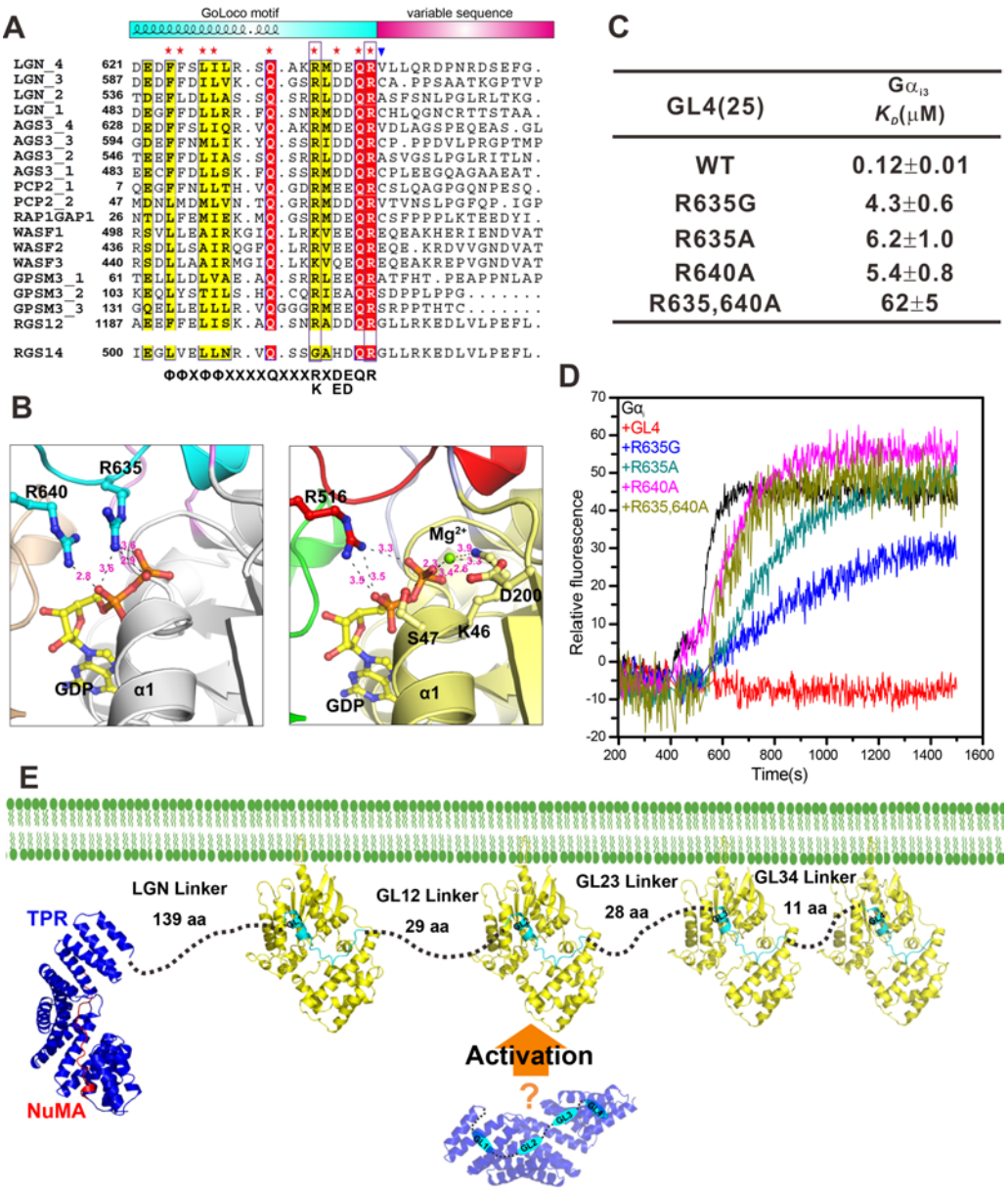
A
GoLoco motif
variable sequence
LGN_4 621 DEDFFSLILR.SQ.AKRMDEQRVLLQRDPNRDSEFG.
LGN_3 587 DEDFFDILVK.CQ.GSRLDDQRCA.PPSAATKGPTVP
LGN_2 536 TDEFLDLLAS.SQ.SRRLDDQRASFSNLPGLRLTKG.
LGN_1 483 DEGFFDLLRR.PQ.SNRMDDQRCHLQGNCRTTSTAA.
AGS3_4 628 DEDFFSLIQR.VQ.AKRMDEQRVDLAGSPEQEAS.GL
AGS3_3 594 GDEFFNMLIK.YQ.SSRIDDQRCP.PPDVLPRGPTMP
AGS3_2 546 TEEFFDLIAS.SQ.SRRLDDQRASVGSLPGLRITLN.
AGS3_1 483 EECFFDLLSK.PQ.SSRMDDQRCPLEEGQAGAAEAT.
PCP2_1 7 QEGFFNLLTH.VQ.GDRMEEQRCSLQAGPGQNPESQ.
PCP2_2 47 MDNLMDMLVN.TQ.GRRMDDQRVTVNSLPGFQP.IGP
RAP1GAP1 26 NTDLFEMIEK.MQ.GSRMDEQRCSFPPPLKTEEDYI.
WASF1 498 RSVLLEAIRKGIQ.LRKVEEQREQEAKHERIENDVAT
WASF2 436 RSDLLSAIRQGFQ.LRRVEEQREQE.KRDVVGNDVAT
WASF3 440 RSDLLAAIRMGIQ.LKKVQEQREQEAKREPVGNDVAT
GPSM3_1 61 TELLLDLVAE.AQ.SRRLEEQRATFHT.PEAPPNLAP
GPSM3_2 103 KEQLYSTILS.HQ.CQRIEAQRSDPPLPPG.......
GPSM3_3 131 GQELLELLLR.VQGGGRMEEQRSRPPTHTC.......
RGS12 1187 AEEFFELISK.AQ.SNRADDQRGLLRKEDLVLPEFL.
RGS14 500 IEGLVELLNR.VQ.SSGAHDQRGLLRKEDLVLPEFL.
ΦΦXΦΦXXXXQXXXRXDEQR
K ED
B
R635
R640
GDP
α1
R516
Mg2+
D200
S47
K46
GDP
α1
C
GL4(25)
Gαi3 Kd(μM)
WT 0.12±0.01
R635G 4.3±0.6
R635A 6.2±1.0
R640A 5.4±0.8
R635,640A 62±5
D
Gαi
+GL4
+R635G
+R635A
+R640A
+R635,640A
Relative fluorescence
Time(s)
E
TPR
NuMA
LGN Linker
139 aa
GL12 Linker
29 aa
GL23 Linker
28 aa
GL34 Linker
11 aa
Activation
?

Figure 6

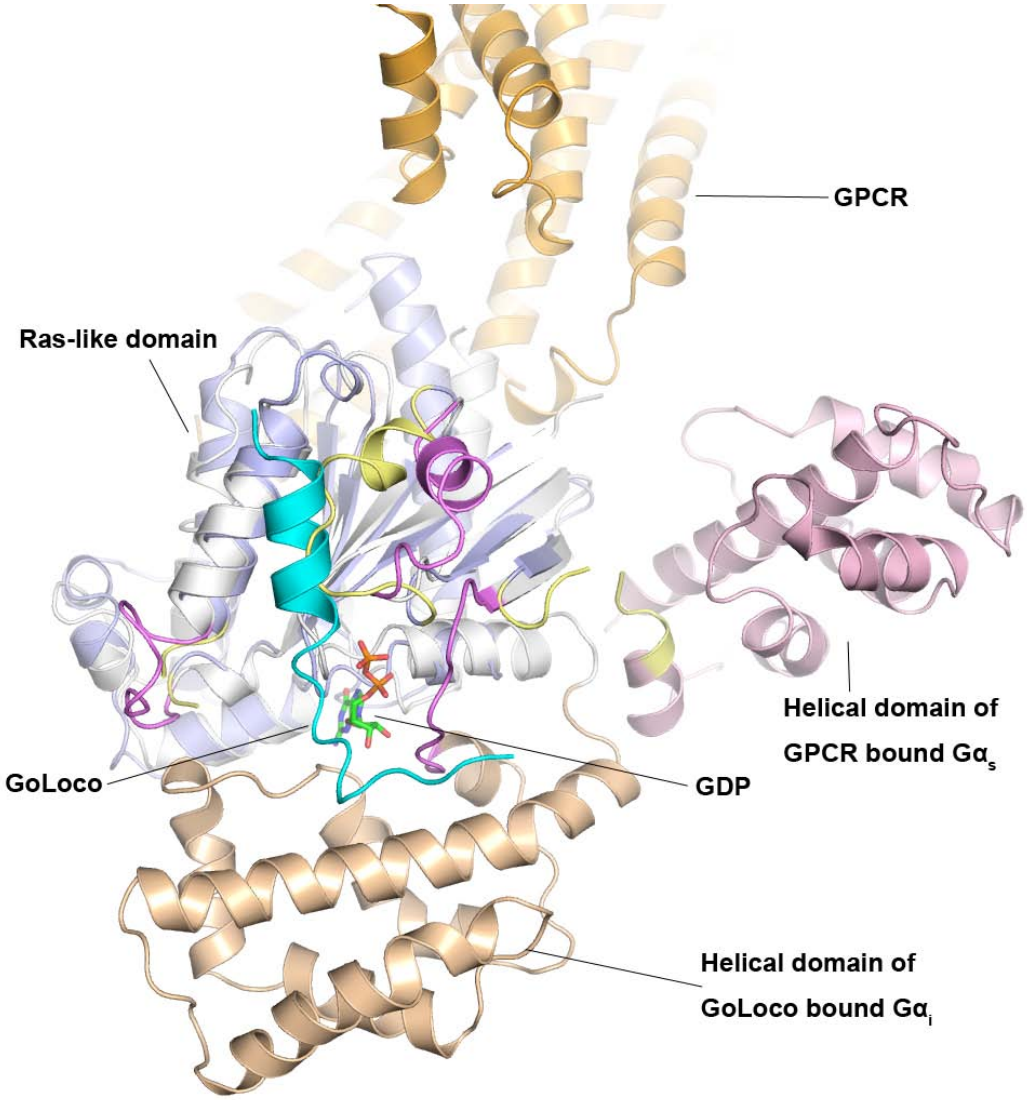
GPCR
Ras-like domain
Helical domain of
GPCR bound Gα$_s$
GoLoco
GDP
Helical domain of
GoLoco bound Gα$_i$

Figure 7